

Quenching mechanism of up-conversion luminescence in glass ceramics containing $\text{Er}^{3+}:\text{NaYF}_4$ nanocrystals

XINGYONG HUANG^{a,b,*}, DAQIN CHEN^c, LIN LIN^d, ZHIQIANG ZHENG^d, HAITAO CHEN^{a,b}, KAI DENG^a

^aSchool of Physics and Electronic Engineering, Yibin University, Yibin Sichuan 644000, China

^bInstitute of Physics, Yibin University, Yibin Sichuan 644000, China

^cFujian Institute of Research on the Structure of Matter, Chinese Academy of Sciences, Fuzhou Fujian 350002, China

^dCollege of Physics and Energy, Fujian Normal University, Fuzhou Fujian 350007, China

The structural and morphological characterizations of the NaYF_4 nanostructured glass ceramic with different concentrations of Er^{3+} are characterized. The red and green up-conversion emission of different samples are measured, respectively. With the increase of the Er^{3+} doping concentration, the green emission intensity first increases, and then decreases, while the red emission intensity continuously rises. Besides, combined with the ratio of the green emission to the red emission and the energy diagram of Er^{3+} ions, the luminescent mechanism of the tunable red-green luminescence is explained. Finally, it's proved that the concentration quenching of green emission is close to an electric dipole-dipole interaction.

(Received September 20, 2013; accepted March 13, 2014)

Keywords: Nano-glass-ceramics, Up-conversion luminescence, Concentration quenching

1. Introduction

Recently, the up-conversion phosphors have been widely applied in solid-state lasers, double photons focus micro-imaging, near-infrared (NIR) quantum cutting devices and biological fluorescent labeling, etc. [1-3]. On the other hand, $\text{Er}^{3+}\text{-Yb}^{3+}$ co-doped NaYF_4 shows that NaYF_4 is currently one of the most efficient hosts for NIR-to-visible up-conversion [4]. Therefore, the rare-earth (RE) doped NaYF_4 phosphor, as an up-conversion material, has shown its great potential application and has been widely studied [5, 6].

However, further applications of NaYF_4 powders have been restricted in many fields such as solid-state laser and optical amplifiers [5,7]. Currently, bulk nanostructured transparent glass ceramics have shown many advantages, such as the excellent optical properties and the convenient and low-cost synthesis [1,8,9]. However, most attention has been focused on the NaYF_4 powders[10-14], and there has been few studies based on NaYF_4 bulk crystal [7]. This is because the bulk single crystal can not be readily grown due to the existing transition between the cubic and hexagonal phases.

In this paper, we report that the up-conversion luminescence can be gradually tuned from green to red with various Er^{3+} concentrations and the inherent mechanism are analyzed in detail. Most importantly, tunable mechanism of upconversion fluorescence also is discussed. The relation of fluorescence integrated intensity and Er-concentration is demonstrated in the atomic interaction.

2. Experimental

The samples were prepared by melt quenching technique using the composition of $40\text{SiO}_2\text{-}25\text{Al}_2\text{O}_3\text{-}18\text{NaCO}_3\text{-}10\text{YF}_3\text{-}7\text{NaF-xErF}_3$ ($x = 0.05, 0.5, 1.0, 2.0$ and 4.0 , respectively, in mol%). All the starting raw materials were highly pure reagents. For each batch, about 15g of original materials were fully mixed. They were then melted in a covered platinum crucible at $1450\text{ }^\circ\text{C}$ for 1 h in the ambient atmosphere to homogenize the melt [5]. Then, the melt was cast into a $400\text{ }^\circ\text{C}$ preheated brass mold followed by annealing at below the glass transition temperature to relinquish the inner stress, and cooled down to room temperature to form the precursor glass [5]. The precursor glass samples with different Er^{3+} doping levels were heat-treated at $620\text{ }^\circ\text{C}$ for 2 h to obtain glass ceramics through controlled crystallization. All samples were cut and polished to flat for the spectroscopic property measurements, and all thickness of the sample was 3.00 mm.

The microstructure images had been carried out on transmission electron microscopy (TEM, JOEL-2010). X-ray diffraction (XRD) analysis was performed with a powder diffractometer (PANalytical X'Pert Pro) to identify the crystallization phase. The red-green were recorded on an InP/InGaAs photomultiplier tubes (PMT, R928). The up-conversion luminescence were measured with exciting light from a 30 mW diode laser. All the measurements were carried out at room temperature.

3. Results and discussions

The XRD characterizations obtained from the

nanostructured glass ceramic are shown in Fig. 1. The XRD pattern displays several sharp diffraction peaks of the cubic phase α - NaYF_4 (JCPDS No. 06-0342). The TEM image of the nanostructured glass ceramic shown in Fig. 2 demonstrates that the spherical crystallites sized 20-25 nm distributes uniformly in the glass matrix, their selected area electron diffraction polycrystalline rings well indexed to the cubic α - NaYF_4 .

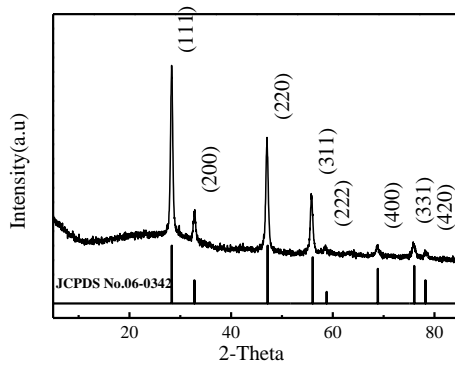


Fig. 1. XRD curves of the nanostructured glass ceramic; the bars represent the diffraction pattern of the standard cubic α - NaYF_4 phase.

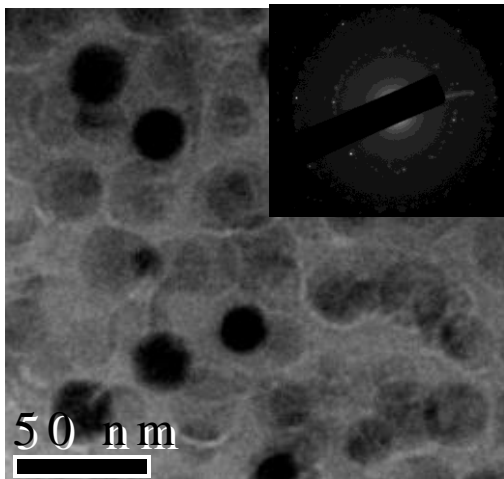


Fig. 2. TEM micrograph and the corresponding selected area electron diffraction pattern of the nanostructured glass ceramic.

The Er^{3+} concentration dependence of red-green up-conversion luminescence under the excitation of a 980 nm diode laser is presented Fig. 3. Two main emission bands have been obviously observed: the green emission peak centered at 545 nm and the red emission peak centered at 660 nm. The fluorescence intensity at 545 nm offer upgrade firstly then descending latter with the increase of Er^{3+} ion concentration, suggesting the existence concentration quenching effect. Meanwhile, red emission intensity continuously rises with increasing the Er^{3+} concentration. The result shows that the larger the concentration of Er^{3+} ions, the further promoted cross-relaxation between ${}^4\text{S}_{3/2}({}^2\text{H}_{11/2}) \rightarrow {}^4\text{I}_{9/2}$ and

${}^4\text{I}_{15/2} \rightarrow {}^4\text{I}_{13/2}$, resulting in decrease of the fluorescence integrated intensity at 545 nm (Er^{3+} concentration ≥ 0.2 mol%). The green light is nearly disappeared as soon as Er^{3+} reaches 2.0 mol%, it should be attributed to the concentration quenching effect.

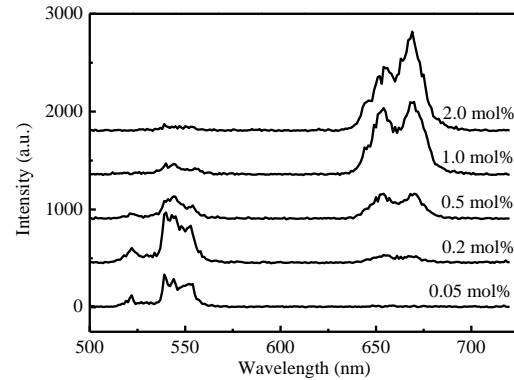


Fig. 3. Up-conversion spectra of the NaYF_4 nanocrystals doped with various concentration of Er^{3+} ions.

Fig. 4 shows the ratio green to red emission intensity, which monotonous reduces with increasing Er^{3+} concentrations. After the atom at ground state can be excited to the level under the excitation at 980 nm, there are fast nonradiative decays to the ${}^4\text{I}_{13/2}$ level. Subsequently, the same laser pumps the excited atom from the ${}^4\text{I}_{13/2}$ level to the ${}^4\text{I}_{9/2}$ level and from the ${}^4\text{I}_{11/2}$ level to the ${}^4\text{F}_{7/2}$ level. These processes are excited state absorption (ESA) and the latter process populate the ${}^4\text{S}_{3/2}({}^2\text{H}_{11/2})$ level. The larger radiative transition probability of ${}^4\text{S}_{3/2}({}^2\text{H}_{11/2})$ determines that the green emission takes an absolute lead in the low doping case. Fluorescence intensity is very weak when the low doping concentration, because there is not enough luminescence center. With increasing Er^{3+} concentrations, there are more luminescence center, which results in red and green fluorescence intensity increased ($x \leq 0.2$ mol%). However, when the doping concentration are increased to the certain extent ($x > 0.2$ mol%), the interaction between Er^{3+} ions are enhanced and the change of the ratio green to red emission can be ascribed to the cross-relaxation between Er^{3+} ions (between ${}^4\text{S}_{3/2}({}^2\text{H}_{11/2}) \rightarrow {}^4\text{I}_{9/2}$ and ${}^4\text{I}_{15/2} \rightarrow {}^4\text{I}_{13/2}$, which weakens the green emission and indirect enhancing the red emission proportion. That is, the closer the rare-earth ions enhance the possibility of cross-relaxation (${}^4\text{S}_{3/2}({}^2\text{H}_{11/2}) + {}^4\text{I}_{15/2} \rightarrow {}^4\text{I}_{9/2} + {}^4\text{I}_{13/2}$ (CR₁); ${}^4\text{I}_{13/2} + {}^4\text{I}_{15/2} \rightarrow {}^4\text{I}_{15/2} + {}^4\text{F}_{9/2}$ (CR₂); ${}^4\text{I}_{9/2} + {}^4\text{I}_{11/2} \rightarrow {}^4\text{I}_{13/2} + {}^4\text{F}_{9/2}$ (CR₃), as presented in Fig. 5). As a result, the populations of ${}^4\text{F}_{9/2}$ level are enhanced and the preponderance of green emission has gradually lost their superiority with the increase of Er^{3+} concentration.

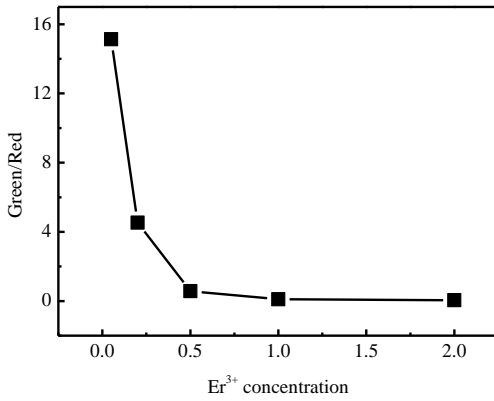


Fig. 4. The ratio of green to red emission intensity with different Er³⁺ doping concentration.

Certainly, CR₂ and CR₃ playing secondary role due to the bigger energy mismatch. However, the distances of Er³⁺ ions are reduced with increasing Er³⁺ concentrations. Results resonant cross relaxation (CR₂ and CR₃) is becoming more and more obvious with the help of the interaction of Er³⁺ ions. These processes enhance the population in ⁴F_{9/2} level [15].

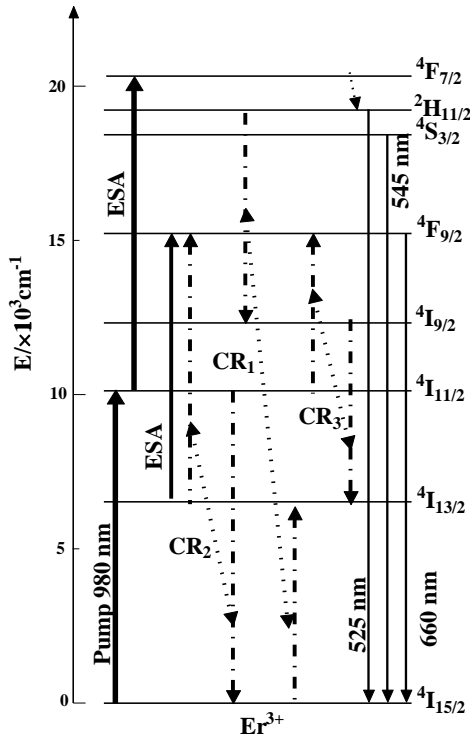


Fig. 5. Energy level diagram of Er³⁺ and up-conversion mechanisms.

From the Huang's previous theoretical study [16, 17], the relationship between the fluorescence integrated intensity (*I*) and the doping concentration (*C*) can be shown that

$$I \propto \{CT(1-d/s)[X_0(1+A)/\gamma]^{d/s}\}^{(1-s/d)} \Gamma(1+s/d) \quad (1)$$

where γ is the intrinsic transition probability of sensitizer (here is activator_itself), and s is the index of electric multipole, which is equal to 6, 8, or 10 for dipole-dipole, dipole-quadrupole, or quadrupole-quadrupole interaction, respectively. If $s=3$, the interaction type is an exchange interaction [17]. d is the dimension of the sample (here d is equal to 3), A and X_0 are constants, and $\Gamma(1+s/d)$ is the gamma function. By logarithmic transformation of Eq. (1), Eq. (1) can be derived that

$$\log(I/C) = -\frac{s}{d} \log C + \log f \quad (2)$$

where f is independent of the concentration. So, just get the relation diagram between $\log(I/C)$ and $\log(C)$, and the slope of lines is equal to $-s/3$ [5]. Then we can determine the interactive types of electric multipole. Fig. 6 shows the $\log(I/C) - \log(C)$ plots for the ⁴S_{3/2}(²H_{11/2}) → ⁴I_{15/2} in the different Er³⁺ doping levels. Good linear fitting are achieved by using Eq. (2) in region of high concentrations, the slope parameters $-s/d$ can be obtained. Fig.6 shows the $\log(I/C) - \log(C)$ plot slope equal to -1.96 (very close to -2). In other words, the index of the electric multipole energy transfer is 6, which implies that the electric dipole-dipole interaction is dominant in this concentration quenching behavior. The quenching mechanism of electric dipole-dipole interaction is dominant in the process of fluorescence integrated intensity decreases.

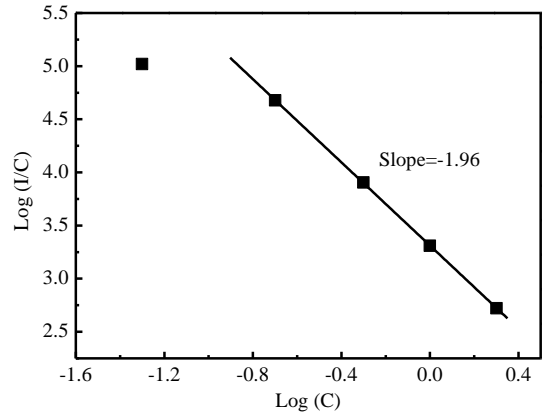


Fig. 6. Log(I/C) – log(C) plot for ⁴S_{3/2}→⁴I_{15/2} transition.

4. Conclusions

The up-conversion fluorescence of Er³⁺ doped NaYF₄ nanostructured glass ceramic has been studied. The prepared samples are identified to be pure cubic phase by the XRD and the spherical crystallites sized 20-25 nm distributed densely and homogeneously are observed by TEM. With various Er³⁺ concentrations, the color of up-conversion fluorescence can be gradually tuned from green to red. The ratio of the green emission to the red

emission intensity is influenced by doping concentration. This phenomenon is due to the cross-relaxation between Er³⁺ ions. The result shows that the quenching mechanism of green emission is an electric dipole-dipole interaction.

Acknowledgements

This work was supported by the National Natural Science Foundation of China (No. 11204039).

References

- [1] F. Liu, E. Ma, D. Q. Chen, Y. L. Yu, Y. S. Wang, J. Phys. Chem. B. **110**, 20843 (2006).
- [2] Y. Jiao, X. Gao, J. Lu, Y. Chen, W. He, X. Chen, X. Li, R. Li, J. Alloy. Compd. **549**, 245 (2013).
- [3] L. Jiang, H. Zhang, S. Xiao, X. Yang, J. Ding, Optoelectron. Adv. Mater. **5**, 547 (2012).
- [4] N. Menyuk, K. Dwight, J. Pierce, Appl. Phys. Lett. **21**, 159 (1972).
- [5] X. Y. Huang, D. Q. Chen, L. Lin, Z. Z. Wang, Y. S. Wang, Z. H. Feng, Z. Q. Zheng, Sci. China-Phys. Mech. Astron. **55**, 1148 (2012).
- [6] Y. Wei, X. Liu, X. Chi, R. Wei, H. Guo, J. Alloy. Compd. **578**, 385 (2013).
- [7] R. H. Page, K. I. Schaffers, P. A. Waide, J. B. Tassano, S. A. Payne, W. F. Krupke, W. K. Bischel, J. Opt. Soc. Am. B. **15**, 996 (1998).
- [8] D. Q. Chen, Y. L. Yu, Y. S. Wang, P. Huang, F. Weng, J. Phys. Chem. C. **113**, 6406 (2009).
- [9] F. Liu, E. Ma, D. Chen, Y. Wang, Y. Yu, P. Huang, J. Alloy. Compd. **467**, 317 (2009).
- [10] J. H. Zeng, J. Su, Z. H. Li, R. X. Yan, Y. D. Li, Adv. Mater. **17**, 2119 (2005).
- [11] N. Martin, P. Boutinaud, M. Malinowski, R. Mahiou, J. Cousseins, J. Alloy. Compd. **275**, 304 (1998).
- [12] S. Heer, K. Kmpe, H. U. Güdel, M. Haase, Adv. Mater. **16**, 2102 (2004).
- [13] K. W. Krämer, D. Biner, G. Frei, H. U. Güdel, M. P. Hehlen, S. R. Lüthi, Chem. Mater. **16**, 1244 (2004).
- [14] J. F. Suyver, J. Grimm, M. K. van Veen, D. Biner, K. W. Krämer, H. U. Güdel, J. Lumin. **117**, 1 (2006).
- [15] R. Balda, A. Oleaga, J. Fernández, J. M. Fdez-Navarro, Opt. Mater. **24**, 83 (2003).
- [16] S. Huang, L. Lou, Chin. J. Lumin. **11**, 1 (1990).
- [17] Q. Meng, B. Chen, W. Xu, Y. Yang, X. Zhao, W. Di, S. Lu, X. Wang, J. Sun, L. Cheng, T. Yu, Y. Peng, J. Appl. Phys. **102**, 093505 (2007).

*Corresponding author: huangxy820@163.com